Chemical Engineering Journal xxx (xxxx) xxx

Contents lists available at ScienceDirect

Chemical Engineering Journal

journal homepage: www.elsevier.com/locate/cej

From biology to biology: Hematoporphyrin-melanin nanoconjugates with synergistic sonodynamic-photothermal effects on malignant tumors

Jiulong Zhang [a,1], Chunzi Shi [a,1], Fei Shan [a,1], Nannan Shi [a], Wen Ye [a], Yaoyao Zhuo [a], Yijun Zhang [a], Zhiyong Zhang [a,*], Yuxin Shi [a,c,*], Chen Peng [a,b,*]

[a] Department of Radiology, Shanghai Public Health Clinical Center, Fudan University, Shanghai 201508, China
[b] Cancer Center, Shanghai Tenth People's Hospital, School of Medicine, Tongji University, Shanghai 200072, China
[c] Shanghai Key Laboratory of Molecular Imaging, Shanghai 201318, China

ARTICLE INFO

Keywords:
Hematoporphyrin
Melanin
Sonodynamic effect
Photothermal therapy
Malignant tumor

ABSTRACT

Compared to the synthetic nanomaterials, the ones modified from biology and capable of multimodal imaging and therapeutic functions have received increasingly interest for tumor theranostics due to their intrinsic biocompatibility and biodegradability. In this work, we firstly prepared the hematoporphyrin-melanin nanoconjugates (HMNCs) whose hematoporphyrin part was originated from the endogenous hemoglobin and melanin part was extracted from the cuttlefish ink. In the case of HMNCs, the hematoporphyrin part could be excited by ultrasound to produce cytotoxic singlet oxygen for sonodynamic therapy (SDT), while the melanin part with strong near-infrared absorbance possessed rapid and efficient photothermal conversion for photothermal therapy (PTT). The in vitro cell experiments confirmed the high biocompatibility of HMNCs, and the combined SDT-PTT achieved much high therapeutical efficacy towards cancer cells in comparison to SDT or PTT alone. Furthermore, in vivo administration of HMNCs at 40 mg kg^{-1} brings no noticeable side effects for mice blood and major organs, showing their high in vivo biosafety. The HMNCs could accumulate in tumor area after intravenously injection so that they provided high contrast for tumor photoacoustic and thermal imaging, and thereafter the tumor growth was highly inhibited through synergistic SDT-PTT in comparison to SDT or PTT alone. Therefore, the HMNCs modified from biology can be served as multifunctional nanoagents for tumor theranostic, and it would inspire to develop novel agents modified from biology and then utilize them for biology.

1. Introduction

Malignant tumors with rapid and uncontrolled growth brings a heavy burden on physical, mental and economic state of patients. To treat these tumors, apart from the clinically used therapeutical approaches, several emerging treatment modalities have been explored by taking advantage of the advanced nanotechnology, such as photosensitizer-based photodynamic therapy [1,2], nutrition-depletion-induced starvation therapy [3,4], nanocarriers-based chemotherapy [5–7], and sonosensitizer-driven sonodynamic therapy (SDT) [8–11] et al. Among these therapies, SDT stands out because it utilizes unharmful ultrasound (US) as the energy source which possesses higher tissue-penetration depth than photodynamic therapy, so that sonosensitizers accumulated within tumor can be efficiently in-situ excited to produce cytotoxic radical oxygen species (ROS) to destroy cancer cells, while bringing a low side-effect for the normal tissue [9]. Currently, a number of sonosensitizers have been prepared which can be basically categorized into inorganic semiconductors (such as TiO_2 nanoparticles [12] and its nanocomposites [13,14]) and organic molecules including hypocrellins [15], protoporphyrin [16], hematoporphyrin [17–19] and et al. However, the therapeutical efficacy of tumor SDT is rather limited by the low oxygen level in solid tumors as well as the short life time (~200 ns) and diffusion distance (<20 nm) of ROS [2]. Therefore, it is urgent to improve the therapeutical efficacy of SDT.

It has been reported that the therapeutical efficacy of SDT can be efficiently enhanced in regard to the improvement of ROS generation or the synergistic effect of multimodal therapeutical functions. In the term of ROS (such as singlet oxygen) generation, it can be boosted by

* Corresponding authors at: Department of Radiology, Shanghai Public Health Clinical Center, Fudan University, Shanghai 201508, China (Z. Zhang, Y. Shi and C. Peng).
E-mail addresses: zhyzhang@fudan.edu.cn (Z. Zhang), shiyuxin@shphc.org.cn (Y. Shi), cpengrr@tongji.edu.cn (C. Peng).
[1] These authors contributed equally to this work.

https://doi.org/10.1016/j.cej.2020.127282
Received 22 July 2020; Received in revised form 12 September 2020; Accepted 4 October 2020
Available online 8 October 2020

enriching the oxygen level within solid tumors through delivering oxygen-carrying bubbles [20,21] and catalyzing the endogenous hydroperoxide into oxygen [22], or facilitating the fast separation of the excited electron-hole pairs by constructing nanocomposites [14,23,24]. For example, Au-TiO_2 nanosheets were prepared by growing Au nanocrystals on the edge of TiO_2 nanosheets and they showed the higher generation efficiency of ROS compared to pure TiO_2 nanosheets, because the high electroconductivity of Au facilitated the separation of the electron-hole pairs from the energy band of TiO_2 nanosheets upon the external US irradiation [14]. Besides the boost of ROS generation, the enhancement of therapeutical efficacy through combing SDT with the other therapeutical modalities is also highly interesting and efficient. Through the rational design of nanoagents, the SDT can be combined with photodynamic therapy (SDT-PDT) [10], chemotherapy (SDT-Chemo) [25], and photothermal therapy (SDT-PTT), and the resulting combined therapy are featured with the synergistic effect. In particular, the SDT-PTT has caught the wide attention and it exhibits higher efficiency in killing cancer cells in vitro and in vivo in comparison to the separate therapy, since the heat can increase the blood flow to enhance ROS generation and the thermosensitivity of cancer cells [26,27]. The nanoagents with sonodynamic and near-infrared (NIR) response are the essence of SDT-PTT, and there are several SDT-PTT nanoagents including lipid nanoparticles loaded with oxygen and indocyanine green [21], black TiO_2@TiO_{2-x} nanoparticles [23], TiO_2-graphene nanocomposites [24], and porphyrin-CuS [28]. It is found that the current SDT-PTT nanoagents are mainly concentrated in non-degradable inorganic sonosensitizers which would remain in the biological system for a very long time and thus causing cytotoxicity concerns, while less attention is paid to organic sonosensitizers. Thus, taking the biocompatibility and biodegradability into consideration, developing SDT-PTT nanoagents with organic component is of highly interest and importance.

Natural melanin is widely distributed in many organisms such as human skin/hair, plant seeds and ink sac of cuttlefish, which contains the active chemical units (such as 5,6-dihydroxyindole-2-carboxylic) with rich amine groups [29,30]. Natural melanin has been recognized as an excellent agent for PTT of tumors because of their native biocompatibility and biodegradability, which could alleviate safety concerns and default metabolism in biological system [31,32]. Given the sonosensitization of hematoporphyrin and the photothermal effect of natural melanin as well as their origin from biology, we firstly prepared the hematoporphyrin-melanin nanoconjugates (HMNCs) by the reaction between the carboxyl groups of hematoporphyrin and amine groups of melanin nanoparticles. These bio-inspired HMNCs were capable of high biocompatibility, US-triggered SDT and NIR laser-induced PTT. Importantly, the combined SDT-PTT achieved much high therapeutical efficacy towards cancer cells in vitro in comparison to SDT or PTT alone. More importantly, when tumor-bearing mice were intravenously injected with HMNCs, HMNCs could accumulate within tumor area to provide high contrast for tumor photoacoustic (PA) and thermal imaging, and then tumor growth was highly inhibited through synergistic SDT-PTT in comparison to SDT or PTT alone, while no obvious side effects could be observed. Therefore, the bio-inspired HMNCs can be served as excellent SDT-PTT nanoagents for tumor theranostics.

2. Experiment section

2.1. Chemicals

Hematoporphyrin (hematoporphyrin monomethyl ether, HMME), Calcein-AM, and propidium iodide (PI) were received from Yuanye Bio-Technology. Natural melanin nanoparticles were harvested from cuttlefish ink and washed heavily with water/ethanol solution. The carboxylated polyethylene glycol (PEG-COOH, *M*w = 5000), dimethyl sulfoxide (DMSO), Indocyanine green (ICG), N-(3-dimethylaminopropyl)-N-ethylcarbodiimide hydrochloride (EDC), 1.3-diphenyl isobenzofuran (DPBF), N-Hydroxysulfosuccinimide (NHS), and 2,2,6,6-Tetramethylpiperidine (TEMP) were brought from Sinopharm Chemical Reagent Co., Ltd. Cell counting kit-8 (CCK-8), 2′,7′-Dichlorofluorescin diacetate (DCFH-DA), and haematoxylin&eosin (H&E) were obtained from Beyotime Biotechnology.

2.2. Preparation of HMNCs

Firstly, EDC (50 mg) and NHS (50 mg) were dissolved into DMSO (5 mL) solution containing hematoporphyrin (20 mg) and PEG-COOH (5 mg), which was stirred for 4 h in the dark. Secondly, the melanin nanoparticles (50 mg) were introduced into above solution, and the mixture was stirred for another 12 h. Thirdly, the above mixture was centrifuged (12000 rpm, 30 min) and the precipitate was washed with water/ethanol (2 mL/8 mL) for three times. The supernatant was collected for testing its absorbance at 396 nm to determine the mass of unreacted hematoporphyrin ($m_{unreacted}$) and reacted hematoporphyrin ($m_{reacted}$ = 20 mg-$m_{unreacted}$). The mass of hematoporphyrin in HMNCs was nearly estimated as $m_{reacted}/(m_{melanin} + m_{reacted}) \times 100\%$.

2.3. Characterizations

The samples were studied by using a JEOL2100 transmission electron microscopy (TEM), a UV-3600 UV–vis-NIR absorption spectrophotometer, a FP-6600 fluorescence spectrometer, an JES-FA200 electron spin resonance (ESR). Hydrodynamic size was measured by using the Zatasizer Nano Z (Malvern).

2.4. Singlet oxygen ($^1O_2$) test

Typically, 5 mg DPBF was dissolved into 5 mL PBS solution to form DPBF solution at 1.0 mg mL^{-1}. Then 40 μL DPBF solution was added into HMNCs in PBS (3 mL, 50 μg mL^{-1}) and exposed to US at 1.75 W cm^{-2}, and the sample was named as (DPBF + HMNCs + US). For comparison, the absorbance changes of (DPBF + US) and (DPBF + Melanin + US) were also measured under the other identical conditions. The absorption spectrum was recorded every 2 min by using UV–vis spectrophotometer. In addition, the ESR signals were collected by introducing TEMP solution (20 μL) into HMNCs or melanin (1 mL, 50 μg mL^{-1}), and then irradiated with US (1.75 W cm^{-2}).

2.5. Photothermal effect

The HMNCs aqueous dispersions (0.1 mL) were added into 0.5 mL plastic tube at a series of concentrations (0, 12.5, 25, 50, 75, and 100 mg mL^{-1}), respectively. Then the plastic tubes containing HMNCs were exposed to an 808 nm NIR laser with the output power of 1.0 W cm^{-2}, and the temperature was captured by a thermal imaging camera.

2.6. Cytotoxicity test

Murine breast cancer 4 T1 cells and human umbilical vein endothelial cells (HUVEC) were grown in DMEM medium under the standard conditions. 4 T1 and HUVEC cells were cultured in 96-well plates (1×10^4/well), and 12 h latter cell medium was discarded and added with a new medium containing HMNCs or melanin at a series of concentrations (0–400 μg mL^{-1}). After 24 h, these cells were washed with PBS and tested by using the standard CCK-8 assay.

2.7. Fluorescence of intracellular HMNCs and $^1O_2$ generation

For the fluorescence of intracellular HMNCs, 4 T1 cells were cultured with HMNCs or melanin at 100 μg mL^{-1} for 6 h, and cells were washed twice and imaged by a digital microscope. For the fluorescence of intracellular $^1O_2$ generation, 4 T1 cells were incubated with HMNCs at 100 μg mL^{-1} for 6 h. Subsequently, cells were cultured with the serum-

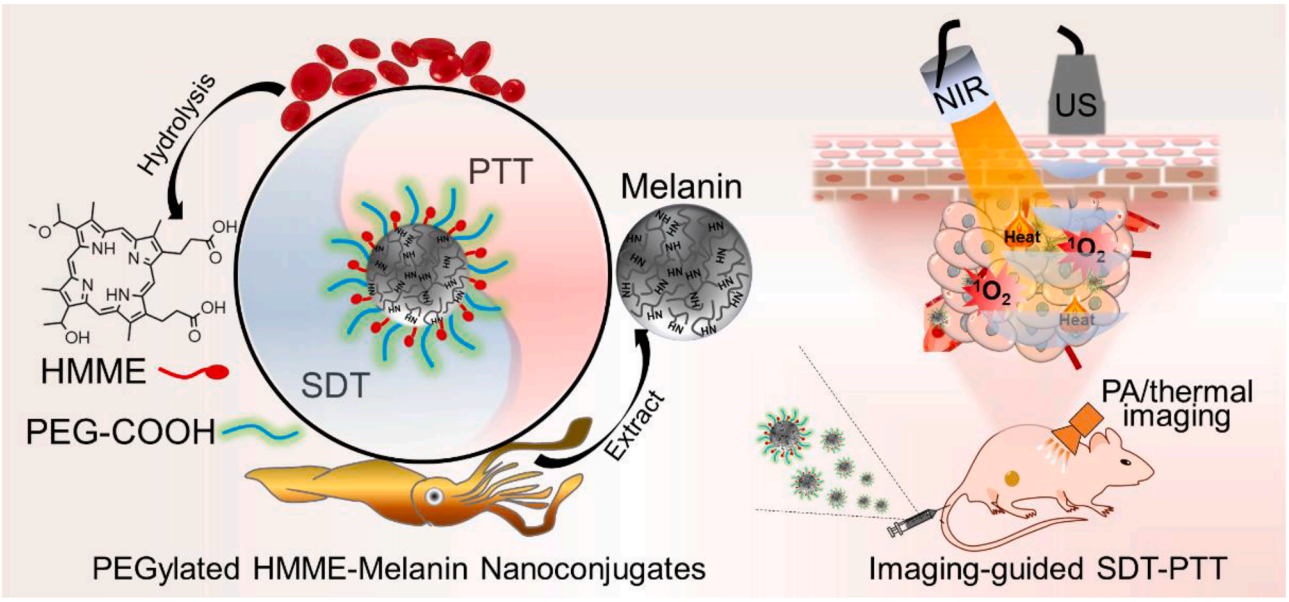

Fig. 1. A scheme illustrating the design of bio-derived HMNCs by conjugating hematoporphyrin and melanin, and their application of imaging-guided synergistic SDT-PTT of malignant tumors.

free medium with DCFH-DA (100 μL, 20 μM). 2 h latter, cells were exposed to US (1.75 W cm^{-2}) for 5 min and imaged.

2.8. Cell therapies

For SDT of 4 T1 cells, they were pre-cultured with HMNCs at 100 μg mL^{-1} for 6 h and illuminated by US for 1, 3, 5, and 7 min, respectively. For PTT of 4 T1 cells, the HMNCs-mediated 4 T1 cells were illuminated with 808 nm NIR laser for different time (3, 5, 7, and 10 min). The US and NIR laser intensity were determined to be 1.75 and 1.0 W cm^{-2}, respectively. For the combined SDT-PTT, 4 T1 cells were cultured with HMNCs at 100 μg mL^{-1} for 6 h and then simultaneously exposed to US and laser for 3, 5, and 7 min, respectively. After irradiation of US and/or NIR laser, the cell viability was evaluated through CCK-8 assay. Meanwhile, cells after same treatments were also performed with Calcine AM/PI assay.

2.9. Blood and histological analysis

Healthy Balb/c mice (n = 3) were intravenously injected with HMNCs saline dispersion (100 μL, 40 mg kg^{-1}), and they were sacrificed at the 30th day. The other three healthy mice were employed (control group). The blood samples were collected for biochemistry analysis, and major organs were cut into slices for H&E staining.

2.10. PA and thermal imaging of tumors

Balb/c mice with 4 T1-tumor (the surface diameter is 0.4–0.5 cm) on the right back were brought from Shanghai SLAC. For PA imaging, tumor-bearing mice were pre-scanned by using a photoacoustic scanner (Endra Nexus 128). Subsequently, the mice were intravenously injected with HMNCs in saline solution (100 μL, 40 mg kg^{-1}) and scanned at a series of post-injection time. For thermal imaging, the mice were intravenously injected with HMNCs saline dispersion (100 μL, 40 mg kg^{-1}) or pure saline (100 μL). At the 6 h post-injection, the tumors were exposed to 808 nm laser at 1.0 W cm^{-2} for 8 min, and the thermal images were recorded.

2.11. Tumor therapies

The tumor-bearing mice were allocated to five groups (n = 5) as following: (I) Control, (II) HMNCs, (III) HMNCs + US, (IV) HMNCs + NIR, and (V) HMNCs + US + NIR. Mice in Group (II-V) were intravenously injected with HMNCs dispersion (100 μL, 40 mg kg^{-1}). Subsequently, the tumor area was respectively exposed to US at 2.5 W cm^{-2} for 5 min (Group III and V) and 808 nm laser at 1.0 W cm^{-2} for 5 min (Group IV and V). After treatments, mice body weight and their tumor volume (length × $width^2$/2) were recorded and calculated every other day. At the 12th day, mice were sacrificed, and the tumors were extracted which further cut into tumor slice for staining with H&E assay.

2.12. Statistical analysis

The data were expressed as the mean value ± standard deviation (SD), and any statistical comparison between two groups was analyzed using the Student's two-tailed *t* test. $^*p < 0.05$, $^{**}p < 0.01$, and $^{***}p < 0.001$.

3. Results and discussion

3.1. The preparation and characterization of HMNCs

The HMNCs were obtained by conjugating hematoporphyrin and PEG-COOH with natural melanin nanoparticles, where hematoporphyrin was used as sonosensitizer for SDT, melanin as a NIR absorber for PTT, and PEG-COOH as a stabilizer for improving hydrophilicity, as demonstrated in Fig. 1. On the one hand, hematoporphyrin part is modified from hemoglobin and it has monomer porphyrins with two carboxyl groups, which is recognized as an efficient sonosensitizer in clinical trials for years [33]. On the other hand, the melanin part is extracted from ink sack of cuttlefish and it is a natural biopolymer that mainly consists of rich amine groups [29]. The conjugation of hematoporphyrin and melanin endows HMNCs with the multimodal imaging ability, US-excited sonodynamic ability and NIR laser-triggered photothermal effect, which can serve as efficient theranostic nanoagents to achieve synergistic SDT-PTT effects on malignant tumors.

The morphology and size of the obtained HMNCs and melanin nanoparticles were firstly investigated by using TEM. After the

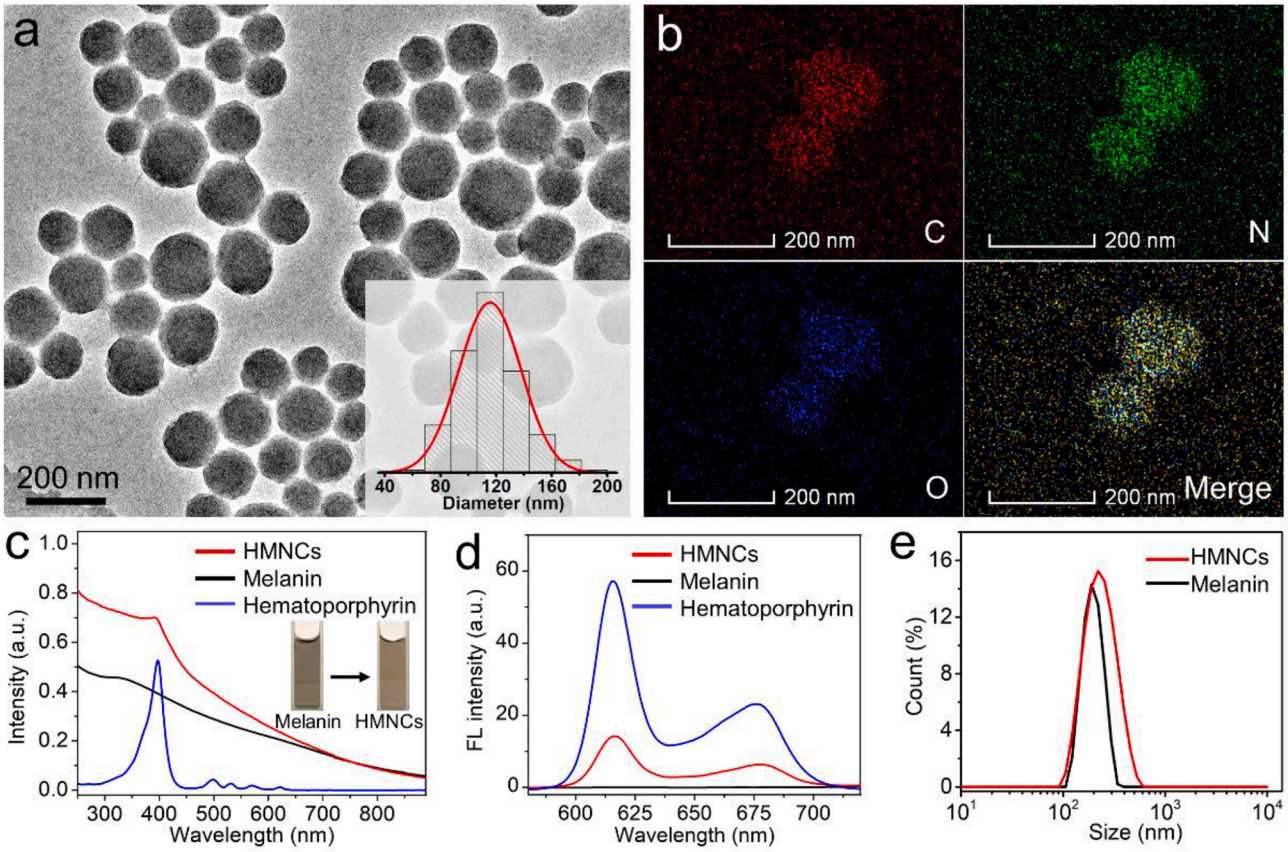

Fig. 2. (a) TEM image and size distribution and (b) elemental maps of HMNCs. (c) UV–vis-NIR absorption spectra and (d) fluorescence spectra of HMNCs, melanin and hematoporphyrin. (e) The hydrodynamic sizes of HMNCs and melanin.

conjugation of hematoporphyrin and PEG-COOH, the HMNCs are prepared and they are composed of the well-defined nanospheres with an average diameter of ~ 115 nm (Fig. 2a), which are same with the morphology of natural melanin nanoparticles extracted from the ink sac of cuttlefish (Fig. S1 in the Supporting Information), indicating the conjugation has no apparent influence on the morphology of melanin nanoparticles. In addition, the elemental map in Fig. 2b shows the strong signal of C/N/O elements that are uniformly distributed within a nanoparticle, which confirm HMNCs are made of C/N/O elements.

Subsequently, the optical properties of HMNCs, natural melanin nanoparticles and hematoporphyrin were studied by using UV–vis-NIR spectrophotometer and fluorescence spectrometer. Natural melanin in deionized water is black and it has a broad and strong photoabsorption ranging from ultraviolet region to NIR region, while hematoporphyrin exhibits the strong absorption band centered at 396 nm (Fig. 2c). Compared to the natural melanin or hematoporphyrin, the HMNCs in deionized water remains black and a strong photoabsorption from 200 to 900 nm, and they show the enhanced absorption intensity in ultraviolet–visible region with a new and broad peak centered at 390 nm. It should be noted that, compared to pure hematoporphyrin, HMNCs manifest the peak shift due to the energy transfer between the hematoporphyrin part and melanin part. The amount of hematoporphyrin in HMNCs is nearly estimated to be around 13.5% by following the equation $m_{reacted}/(m_{melanin} + m_{reacted}) \times 100\%$, where $m_{reacted}$ and $m_{melanin}$ represent the mass of reacted hematoporphyrin and melanin nanoparticles, respectively. Moreover, under the excitation of 400 nm, the HMNCs in deionized water exhibit strong fluorescence with two emission peaks respectively positioned at 616 and 678 nm in comparison to the non-fluorescence of natural melanin, and their fluorescence intensity goes down obviously because of energy transfer from the hematoporphyrin part to the melanin part (Fig. 2d). In addition, the average hydrodynamic size of HMNCs is determined to be 220 nm, which is larger than that (190 nm) for melanin nanoparticles (Fig. 2e). It is also found that the zeta potential changes from + 16.8 mV for melanin to + 2.7 mV for HMNCs. In addition, after storing at ambient condition for one week, the nanoconjugates without PEGylation in deionized water exhibited aggregation while no obvious aggregation would be found for melanin and PEGylated HMNCs (Fig. S2), indicating the high water-stability of PEGylated HMNCs. Together with the above results, we can confirm that the successful preparation of HMNCs with high water stability.

3.2. Sonodynamic and photothermal properties

The HMNCs contain hematoporphyrin and melanin, in which the hematoporphyrin part can be excited by US to transform neighboring O_2 into cytotoxic $^1O_2$ and the melanin part can be stimulated by NIR laser to convert laser energy into heat (Fig. 3a). For the detection of US-triggered generation of $^1O_2$, the DPBF was added into HMNCs dispersion (50 μg mL^{-1}). Under the excitation of US, the intensity of absorption band of DPBF goes down continuously as increasing the excitation time, indicating the generation of $^1O_2$ by HMNCs with US (Fig. 3b). It has been revealed that 51% of DPBF is oxidized in HMNCs dispersion after 10 min of irradiation, while no obvious reduction in absorption intensity in pure DPBF solution or the melanin-mediated DPBF solution (Fig. 3c). Furthermore, the ESR analysis (Fig. 3d) demonstrates the strong signal for TEMP solution containing HMNCs after US for 5 min, whereas no noticeable signal can be observed for TEMP solution of melanin with US. Therefore, the above results solidly confirm the generation of $^1O_2$ that can only be achieved by the combination of HMNCs and US exposure.

After demonstrating $^1O_2$ generation capacity, we investigated the photoabsorption and photothermal effect of HMNCs. The aqueous

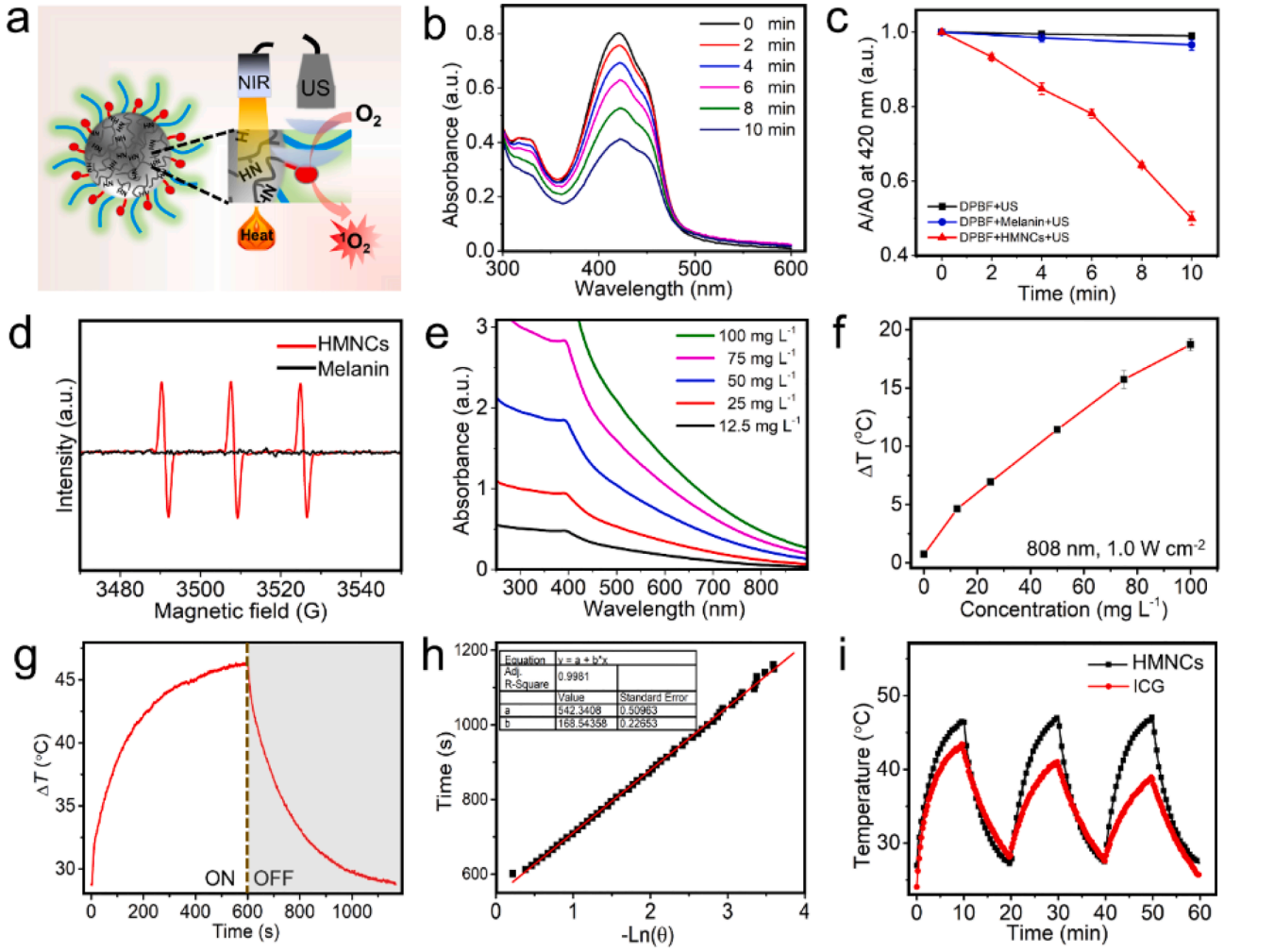

Fig. 3. (a) The scheme showing US-triggered $^1O_2$ generation and NIR laser-driven photothermal effect from HMNCs. (b) The absorption of HMNCs-treated DPBF with US (1.75 W cm^{-2}). (c) The oxidation performance of DPBF with different conditions. (d) ESR signal of TEMP mediated with HMNCs or melanin upon US. (e) UV–vis-NIR absorption spectra of HMNCs dispersions at a series of concentrations. (f) Temperature elevation (ΔT) of HMNCs aqueous dispersions after laser irradiation for 5 min. (g) Temperature curve of HMNCs aqueous dispersion responded to 808 nm laser on/off. (h) Linear time data versus -ln(θ) obtained after NIR laser off. (i) Temperature changes of HMNCs and ICG during three irradiation cycles.

solutions containing HMNCs (12.5–100 μg mL^{-1}) exhibit the enhanced photoabsorption intensity, and the absorbance at 808 nm lineally goes up with the concentration (Fig. 3e and S3). When exposed to an 808 nm laser at 1.0 W cm^{-2}, these dispersions can response to laser irradiation with rapid temperature elevation, while the temperature of deionized water elevates only 1.6 °C. After 300 s of continuous irradiation, the temperature elevations (ΔT) of HMNCs aqueous dispersions are determined to be 4.6, 6.9, 11.4, 15.7, and 18.7 °C at 12.5, 25, 50, 75, and 100 μg mL^{-1}, respectively (Fig. 3f), showing the strong and concentration-relied photothermal effect of HMNCs.

To further delineate on photothermal effect of HMNCs, we calculated the photothermal conversion efficiency (η) [34]. The HMNCs aqueous dispersion with the concentration of 75 μg mL^{-1} was continuously irradiated with an 808 nm laser for 10 min to allow the reach of temperature equilibrium. Fig. 3g shows the temperature curve of HMNCs during laser on/off process, in which the temperature goes up from 28.7 °C to the balanced temperature of 46.4 °C. Fig. 3h manifests the calculation of the system time constant τs as 168.5 s, other specific parameters are supplied in Table S1. The η is determined to be 40.6% which is comparable to the reported melanin nanoparticles and dopamine nanoparticles [35,36]. In addition, the laser stability of HMNCs was also investigated by comparing with ICG dye. Upon irradiation, the maximin temperature for HMNCs dispersion is stabilized at 47 ± 2 °C during three irradiation cycles with 10 min irradiation of each cycle, whereas the maximin temperature of ICG solution shows obvious reduction from 43.7 at the first cycle to 39.1 °C at the third cycle (Fig. 3i). The rapid and efficient photothermal conversion as well as high NIR stability enable HMNCs with great potential in PTT application.

3.3. *The cytotoxicity and therapies in vitro*

Hematoporphyrin is originated from endogenous hemoglobin and natural melanin is biosynthetic nanoparticles by cuttlefish, and they have been recognized to be high biocompatible. For HMNCs and melanin, their cytotoxicity tests were carried out on cell lines of 4 T1 and HUVEC. After 24 h of incubation, 4 T1 and HUVEC cells remain high activity with the average viability of more than 85% at 0–600 μg mL^{-1}, verifying high biocompatibility of HMNCs and melanin (Fig. 4a). Subsequently, the intracellular localization of HMNCs was studied by incubating cells with HMNCs (100 μg mL^{-1}), and then imaged under the excitation of 408 nm. Compared with the melanin-cultured cells in the absence of red fluorescence, the HMNCs-treated cells demonstrate the strong red fluorescence in cytoplasm, which confirms the internalization of HMNCs (Fig. 4b). As the result of internalization, HMNCs can produce singlet oxygen ($^1O_2$) within cells under the irradiation of US, and the intracellular $^1O_2$ can be detected by using green-emitting DCFH which is

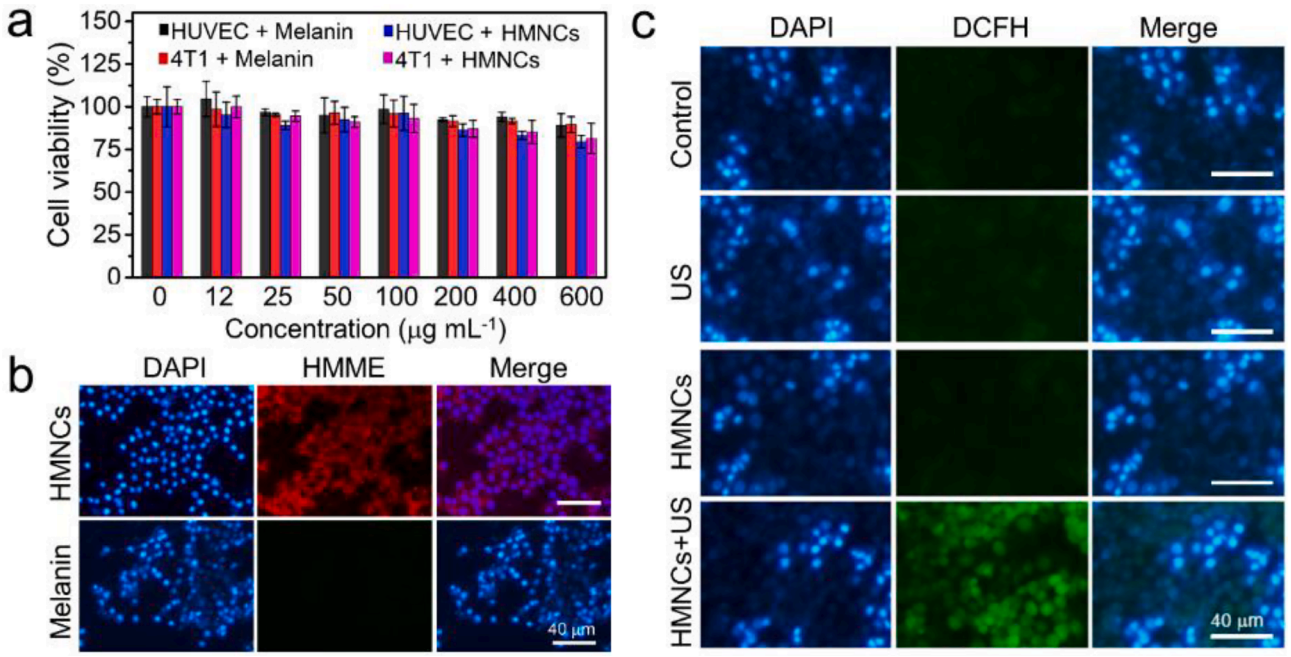

Fig. 4. (a) Cytotoxicity of HMNCs and melanin on 4 T1 and HUVEC cells. (b) Fluorescence images of DAPI-stained 4 T1 cells after the incubation with HMNCs or melanin. (c) Fluorescence images of DCFH-DA/DAPI co-stained 4 T1 cells after treatments.

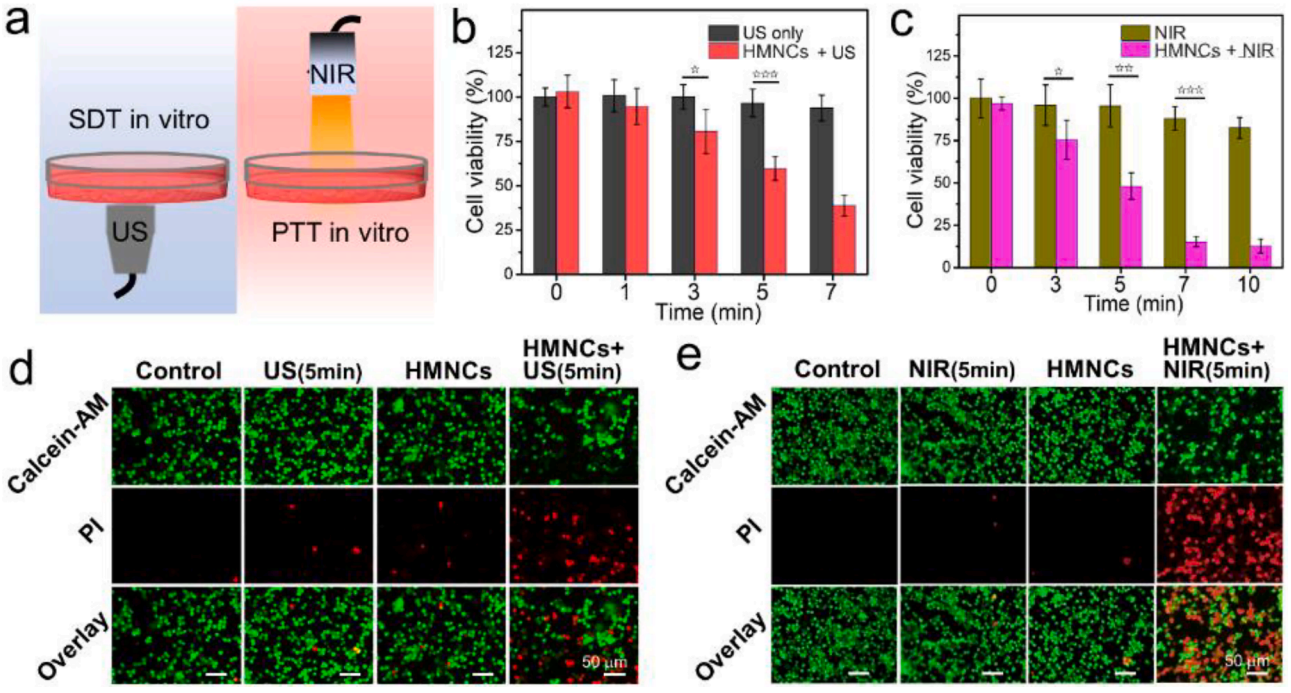

Fig. 5. (a) The setup showing SDT or PTT of 4 T1 cells in vitro. (b) Viability of Cells treated with or without HMNCs (100 μg mL^{-1}) upon US for different time. (c) Viability of Cells incubated with or without HMNCs and laser for different irradiation time. (d, e) Fluorescence images of the treated 4 T1 cells stained with Calcein AM/ PI.

oxidization product of DCFH-DA dye. As shown in fluorescence image (Fig. 4c), 4 T1 cells incubated with HMNCs and US (1.75 W cm^{-2}, 5 min) exhibit bright green fluorescence in comparison to negligible fluorescence for cells received HMNCs or US alone. Thus, the HMNCs with high biocompatibility can be internalized into cells and generates $^1O_2$ upon US irradiation.

Subsequently, the SDT or PTT in vitro were examined separately and the setup was illustrated in Fig. 5a. For SDT in vitro, the US (1.75 W cm^{-2}) was applied to irradiate cells from the down surface with the gel between US transducer and cell plate. When 4 T1 cells were exposed to US, there is no obvious difference in cell viability with increasing exposure time up to 7 min. Once US irradiation is applied for HMNCs-mediated cells, the viability significantly goes down and it is determined to 80%, 59%, or 38% for 3, 5, or 7 min of irradiation in comparison to their parallel group, respectively (Fig. 5b). In the term of PTT in vitro, 808 nm laser at 1.0 W cm^{-2} was employed to illuminate cells

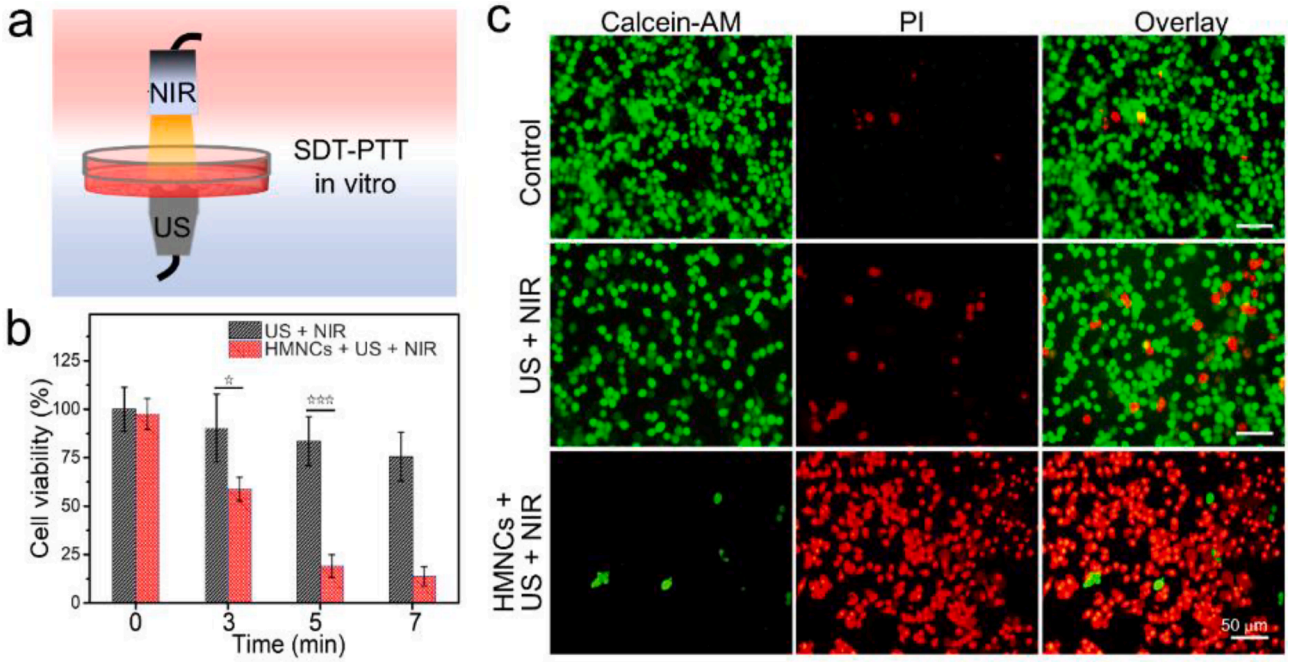

Fig. 6. (a) The setup for SDT-PTT. (b) The viability of cells with or without HMNCs exposed to US (1.75 W cm^{-2}, 5 min) and/or laser (1.0 W cm^{-2}, 5 min). (c) The fluorescence images of the treated cells stained with Calcein AM/PI assay.

from top surface. Under the irradiation of NIR laser, 4 T1 cells in the absence of HMNCs show a slight reduction in viability, indicating NIR laser alone unable to produce enough heat to kill cancer cells (Fig. 5c). On the contrary, when 4 T1 cells treated with both HMNCs and NIR laser, the viability decreases to 75%, 48%, or 15% for irradiation time of 3, 5, or 7 min in contrast to their parallel group, respectively. The continuous reduction of cell viability indicates that the longer irradiation time can convert more heat to confer higher temperature, so as to thermally ablate more cells. Therefore, we can achieve the variable therapeutical efficiency towards cancer cells by simply tuning the treatment time of US or NIR laser.

To visualize the therapeutical efficacy, 4 T1 cells after treatments

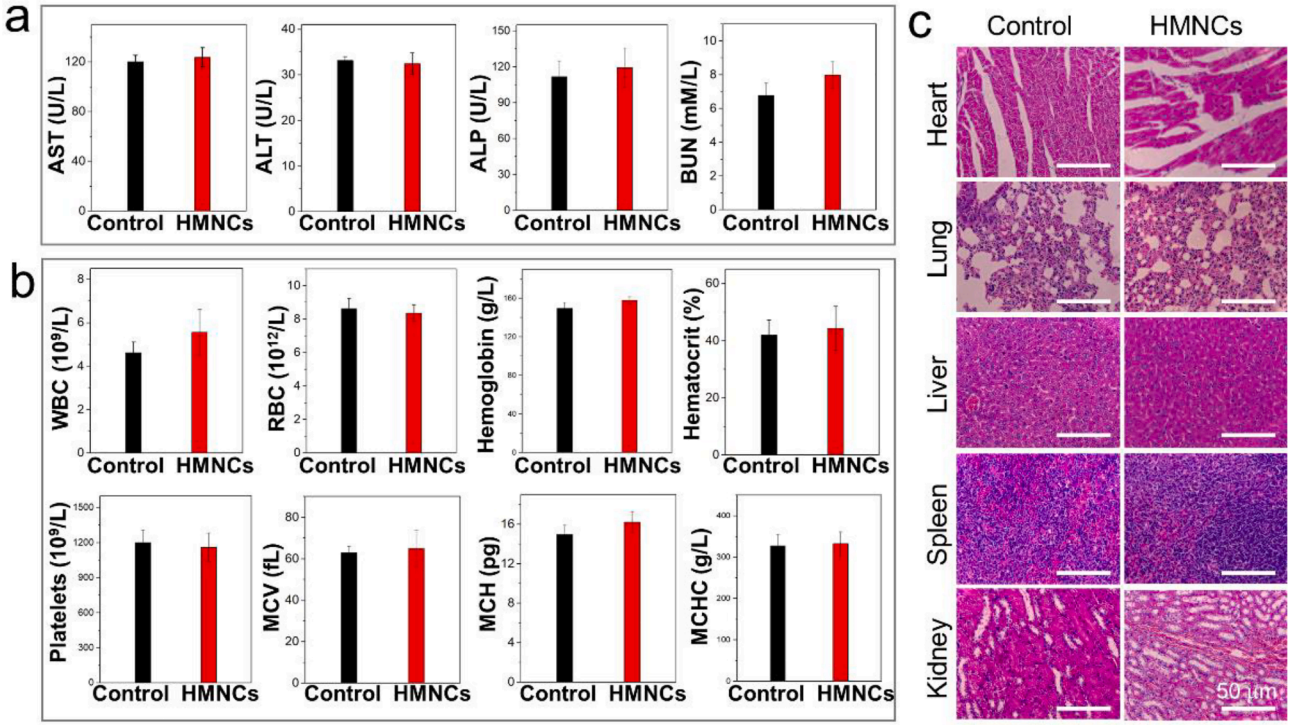

Fig. 7. (a) Blood biochemistry, (b) hematology data, and (c) H&E-stained organ slices of healthy mice injected with HMNCs dispersion or saline solution after 30 days. Aspartate aminotransferase (AST), Alanine aminotransferase (ALT), Alkaline phosphatase (ALP), Blood urea nitrogen (BUN), White blood cells (WBC), Red blood cells (RBC), Mean corpuscular volume (MCV), Mean corpuscular hemoglobin (MCH), and Mean corpuscular hemoglobin concentration (MCHC). (For interpretation of the references to colour in this figure legend, the reader is referred to the web version of this article.)

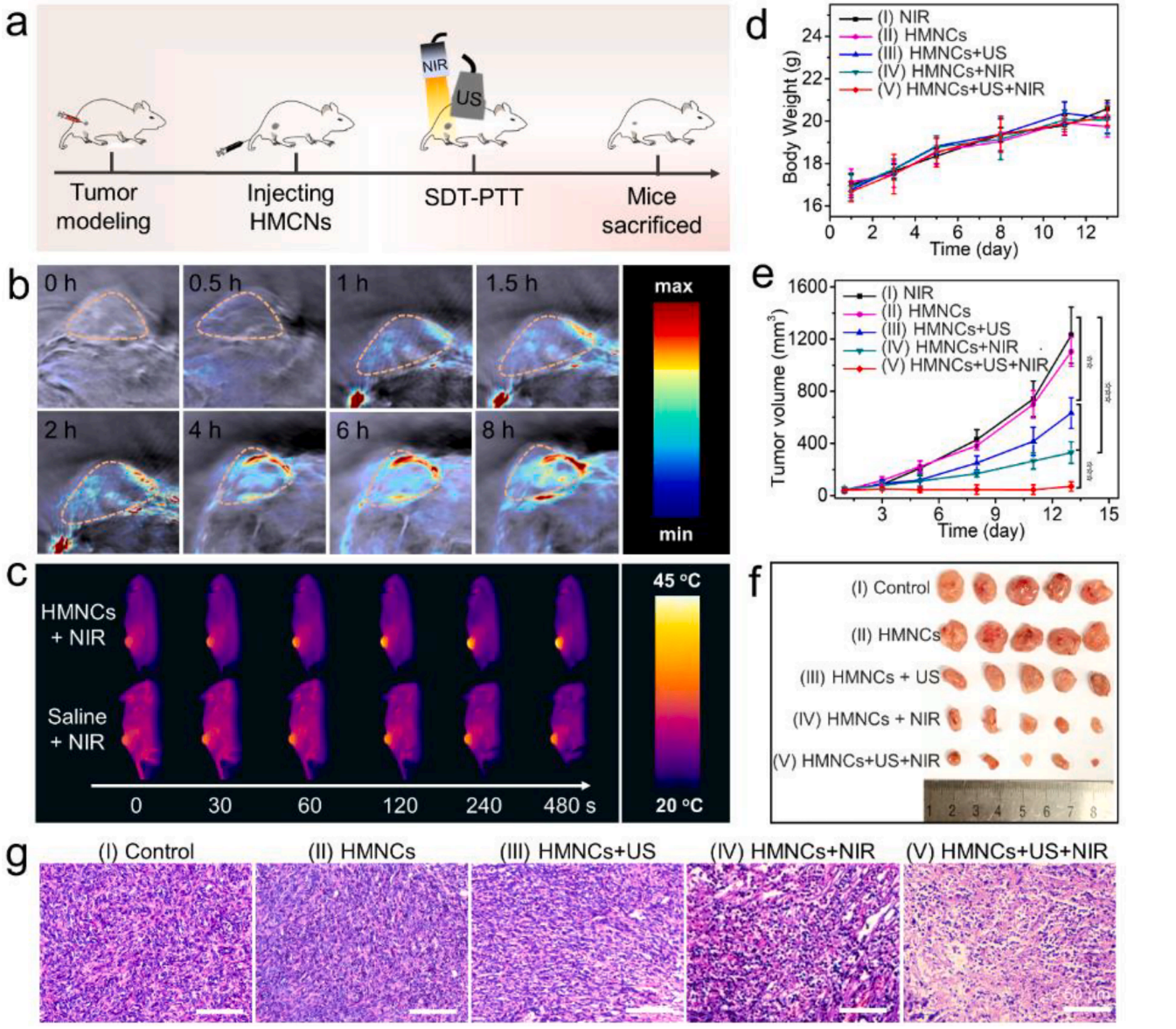

Fig. 8. (a) Schematic of imaging-guided SDT-PTT on 4 T1 tumor-bearing mice. (b) Temporal PA imaging of tumor area at pre- and post-injection of HMNCs. (c) The thermal image of mice treated with HMNCs or saline solution exposed to laser. (d) Mice weight and (e) tumor growth curves after various treatments. (f) Photograph of tumors harvested for the sacrificed mice. (g) H&E-stained images of reprehensive tumor slices.

were stained with Calcein AM/PI assay. When cells are treated with HMNCs or US for 5 min, nearly all of cells manifest green fluorescence which is same as the fluorescence image of cells in the control group (without treatment), implying high activity of these cells under the given condition (Fig. 5d). On the contrary, after incubated with HMNCs for 4 h and then irradiated with US for 5 min, part of cells is destroyed and appear with red fluorescence. Similarly, the strong red fluorescence can be observed only for cells treated with HMNCs and 808 nm laser for 5 min, indicating these cells are thermally ablated by the photothermal effect, while nearly whole green fluorescence is found for cells in other groups (Fig. 5e). Thus, it is concluded that, given 5 min of irradiation of US or NIR laser, neither PTT nor SDT unable to completely kill cancer cells, showing the limited therapeutical efficacy of the separate therapy.

After investigating SDT and PTT in vitro separately, we carried out SDT-PTT by simultaneously utilizing 808 nm laser from top surface and US from down surface under the other identical conditions, as shown in the scheme in Fig. 6a. The effect of therapy time on cell viability is examined and the resulting CCK-8 results reveal that, after treated with both US and laser, the viability of cells without HMNCs also go down from 90% to 75% as increasing the treatment time from 3 to 7 min (Fig. 6b). For the HMNCs-incubated cells, the combined therapy of SDT-PTT can efficiently destroy 4 T1 cells at the highly significance (versus control group, $P < 0.001$) for 5 min. Meanwhile, cells after SDT-PTT for 5 min were co-stained with Calcein-AM and PI staining assay. Apparently, red fluorescence overwhelmingly occupies almost all of cells after receiving HMNCs and SDT-PTT, while cells in other groups mainly present green fluorescence (Fig. 6c). Therefore, the combined SDT-PTT can achieve high therapeutical efficacy in comparison to SDT or PTT alone.

3.4. The biosafety and therapies in vivo

Prior to in vivo experiments, the biosafety in vivo was studied by i.v. injecting HMNCs saline dispersions (100 μL, 40 mg kg^{-1}) or saline solution (100 μL) into health Balb/c mice, respectively. The behavior of mice was as usual, and mice were sacrificed for blood and histological examination at the 30th day. For blood test, there is no notable difference between HMNCs and saline administration regarding blood

biochemistry and hematology, such as liver function markers (such as AST) and the number of white/red blood cells (Fig. 7a, b). Furthermore, the major organs were cut into slice and stained with H&E assay. As shown in Fig. 7c, the H&E-stained organ slices exhibit the normal histological morphology, implying the normal functions of organs. Therefore, the HMNCs at the given concentration have the satisfactory long-time biosecurity.

It has been widely accepted that imaging technologies are highly important to improve the tumor therapeutic efficacy and minimize side effects [37]. In order to guide SDT-PTT of tumors (Fig. 8a), we explored the imaging potential of HMNCs on tumor-bearing mice. It has been widely reported that NIR-responsive materials can be employed as contrast agents for PA imaging with high penetration depth and good spatial resolution [38–40]. Owing to the strong photothermal effect, the melanin nanoparticles have been proved to be an efficient PA imaging agent and they exhibit high contrast for tumor tissue with melanin accumulation [32,41]. To demonstrate the tumor PA imaging capacity, the HMNCs saline dispersion (100 μL, 40 mg kg^{-1}) was i.v. administrated and tumor area was scanned by using photoacoustic computed tomography scanner. Obviously, the tumor area is relatively dark at pre-injection, and it becomes more and more bright at post-injection (Fig. 8b). Correspondingly, the PA signal intensities of tumor area are determined and the intensity at 6 h post-injection is ~5-time higher than that at pre-injection (Fig. S4). In addition, the thermal imaging of tumors was also performed through intravenously injecting HMNCs saline dispersion (100 μL, 40 mg kg^{-1}) or saline solution (100 μL) and then irradiating tumor area with laser (1.0 W cm^{-2}) at the 6 h post-injection. During the irradiation, the tumor area of HMNCs-injected mouse becomes much bright and the temperature of tumor surface increases from 34.6 °C to the balanced temperature of around 45 °C which can induce mild PTT effect (Fig. S5). In contrast, the temperature of tumor surface goes up only 2.6 °C for saline-injected mouse. Therefore, it is confirmed that HMNCs can accumulated within tumor and thus conferring to PA and thermal imaging of tumors.

Under the guide of tumor imaging, the SDT-PTT was proceeded on 4 T1 tumor-bearing mice at the 6 h post-injection and its therapeutical efficiency was evaluated by comparing to SDT or PTT alone. The mice bearing with 4 T1 tumor were allocated to five groups: (I) Control, (II) HMNCs, (III) HMNCs + US, (IV) HM-PEG + NIR, and (V) HMNCs + US + NIR. After different treatments, the weight of mice body and the volume of tumors were recorded and calculated. It has been found that there is no loss in body weight for mice in all groups over a period of 13 days (Fig. 8d). The volume profile in Fig. 8e shows the closed growth rate of tumors between group (I) and group (II), suggesting no noticeable therapeutical ability by only injection of HMNCs. For tumors in group (III and IV), their growth is obvious inhibited at moderate significance (versus group (I), $p < 0.01$) after SDT and high significance (versus group (I), $p < 0.001$) after PTT, respectively. For the SDT-PTT, the growth rate of tumors in group (V) is highly ($p < 0.001$) inhibited compared to group (III and IV), verifying high therapeutical effect.

Subsequently, mice were sacrificed, and tumors were extracted. The photograph of tumors is shown in Fig. 8f, which clearly manifests the smallest tumor size in group (V) among the other groups. Additionally, Fig. S6 summarizes the weight of tumors for each group, and the average tumor weights are determined to be 0.48, 0.47, 0.28, 0.13, 0.06 g for group (I, II, III, IV, and V), respectively. The tumor inhibitory rate was calculated by following the equation $(1\text{-}TW_{treatment}/TW_{control}) \times 100\%$, where $TW_{treatment}$ and $TW_{control}$ stand for the average tumor weight of treatment groups and control group. Therefore, the tumor inhibitory rates are respectively determined to be 87.5%, 72.9%, and 41.7% for SDT-PTT, SDT, and PTT. Furthermore, among the typical images of H&E-stained tumor slices, tumor cells in group (IV and V) show the obvious morphology destruction and the condensed nuclei (Fig. 8g). Therefore, the above results prove that SDT-PTT can achieve the higher therapeutical effect than PTT or SDT alone.

4. Conclusions

In summary, the bio-inspired HMNCs theranostic agents have been prepared by conjugating hematoporphyrin with natural melanin nanoparticles. The HMNCs exhibited sonodynamic and photothermal effect, which efficient produced $^1O_2$ under the excitation of US as well as rapidly converted NIR laser energy into heat with the conversion efficiency of 40.6%. The HMNCs had high biocompatibility and were internalized within cancer cells. When HMNCs were incubated with cancer cells in vitro and treated with US and/or NIR laser, the combined SDT-PDT could achieve high therapeutical efficacy in comparison to SDT or PTT alone. In addition, with the blood and histological safety, HMNCs were i.v. administrated into mice model and they accumulated in tumor for high contrast tumor PA and thermal imaging. Furthermore, compared to the limited therapeutical effect from SDT or PTT alone, the SDT-PTT can highly inhibit tumor growth rate. Therefore, this work prepared the bio-inspired HMNCs as biocompatible and efficient theranostic nanoagents for tumor therapy, and it would inspire to develop other novel nanoagents modified from biology and then utilizing them for biology.

Declaration of Competing Interest

The authors declare that they have no known competing financial interests or personal relationships that could have appeared to influence the work reported in this paper.

Acknowledgements

This work was financially supported by Shanghai Public Health Clinical Center (KY-GW-2020-19) and Shanghai Science and Technology Committee (No. 20441900600).

Appendix A. Supplementary data

Supplementary data to this article can be found online at https://doi.org/10.1016/j.cej.2020.127282.

References

[1] L. Huang, Z. Li, Y. Zhao, Y. Zhang, S. Wu, J. Zhao, G. Han, Ultralow-power near infrared lamp light operable targeted organic nanoparticle photodynamic therapy, J. Am. Chem. Soc. 138 (2016) 14586–14591.
[2] W.P. Fan, P. Huang, X.Y. Chen, Overcoming the Achilles' heel of photodynamic therapy, Chem. Soc. Rev. 45 (2016) 6488–6519.
[3] C. Zhang, D.L. Ni, Y.Y. Liu, H.L. Yao, W.B. Bu, J.L. Shi, Magnesium silicide nanoparticles as a deoxygenation agent for cancer starvation therapy, Nat. Nanotech. 12 (2017) 378–386.
[4] R. Zhang, L. Feng, Z. Dong, L. Wang, C. Liang, J. Chen, Q. Ma, R. Zhang, Q. Chen, Y. Wang, Z. Liu, Glucose & oxygen exhausting liposomes for combined cancer starvation and hypoxia-activated therapy, Biomaterials. 162 (2018) 123–131.
[5] C. Du, Y. Ding, J. Qian, R. Zhang, C.-M. Dong, Achieving traceless ablation of solid tumors without recurrence by mild photothermal-chemotherapy of triple stimuli-responsive polymer–drug conjugate nanoparticles, J. Mater. Chem. B. 7 (2019) 415–432.
[6] Y. Ding, C. Du, J. Qian, C.-M. Dong, NIR-responsive polypeptide nanocomposite generates NO gas, mild photothermia, and chemotherapy to reverse multidrug-resistant cancer, Nano Lett. 19 (2019) 4362–4370.
[7] S. Gao, G. Tang, D. Hua, R. Xiong, J. Han, S. Jiang, Q. Zhang, C. Huang, Stimuli-responsive bio-based polymeric systems and their applications, J. Mater. Chem. B. 7 (2019) 709–729.
[8] K. Su, L. Tan, X. Liu, Z. Cui, Y. Zheng, B. Li, Y. Han, Z. Li, S. Zhu, Y. Liang, X. Feng, X. Wang, S. Wu, Rapid photo-sonotherapy for clinical treatment of bacterial infected bone implants by creating oxygen deficiency using sulfur doping, ACS Nano. 14 (2020) 2077–2089.
[9] S. Kwon, H. Ko, D.G. You, K. Kataoka, J.H. Park, Nanomedicines for reactive oxygen species mediated approach: An emerging paradigm for cancer treatment, Acc. Chem. Res. 52 (2019) 1771–1782.
[10] Z. Liu, J. Li, W. Chen, L. Liu, F. Yu, Light and sound to trigger the Pandora's box against breast cancer: A combination strategy of sonodynamic, photodynamic and photothermal therapies, Biomaterials. 232 (2020), 119685.
[11] J. Li, A. Xi, H. Qiao, Z. Liu, Ultrasound-mediated diagnostic imaging and advanced treatment with multifunctional micro/nanobubbles, Cancer Lett. 475 (2020) 92–98.

[12] Y. Harada, K. Ogawa, Y. Irie, H. Endo, L.B. Feril, T. Uemura, K. Tachibana, Ultrasound activation of TiO_2 in melanoma tumors, J. Control. Release. 149 (2011) 190–195.
[13] V.G. Deepagan, D.G. You, W. Um, H. Ko, S. Kwon, K.Y. Choi, G.R. Yi, J.Y. Lee, D. S. Lee, K. Kim, I.C. Kwon, J.H. Park, Long-circulating Au-TiO_2 nanocomposite as a sonosensitizer for ROS-mediated eradication of cancer, Nano Lett. 16 (2016) 6257–6264.
[14] Y. Cao, T. Wu, W. Dai, H. Dong, X. Zhang, TiO_2 nanosheets with the Au nanocrystal-decorated edge for mitochondria-targeting enhanced sonodynamic therapy, Chem. Mater. 31 (2019) 9105–9114.
[15] X. Zheng, W. Liu, J. Ge, Q. Jia, F. Nan, Y. Ding, J. Wu, W. Zhang, C.S. Lee, P. Wang, Biodegradable natural product-based nanoparticles for near-infrared fluorescence imaging-guided sonodynamic therapy, ACS Appl. Mater. Inter. 11 (2019) 18178–18185.
[16] H. Zhang, Q. Li, R. Liu, X. Zhang, Z. Li, Y. Luan, A versatile prodrug strategy to in situ encapsulate drugs in mof nanocarriers: A case of cytarabine-IR820 prodrug encapsulated ZIF-8 toward chemo-photothermal therapy, Adv. Funct. Mater. 28 (2018) 1802830.
[17] X. Ding, Q. Xu, F. Liu, P. Zhou, Y. Gu, J. Zeng, J. An, W. Dai, X. Li, Hematoporphyrin monomethyl ether photodynamic damage on hela cells by means of reactive oxygen species production and cytosolic free calcium concentration elevation, Cancer Lett. 216 (2004) 43–54.
[18] H. Zhang, X. Zhang, Y. Ren, F. Cao, L. Hou, Z. Zhang, An in situ microenvironmental nano-regulator to inhibit the proliferation and metastasis of 4T1 tumor, Theranostics. 9 (2019) 3580–3594.
[19] W. Yue, L. Chen, L. Yu, B. Zhou, H. Yin, W. Ren, C. Liu, L. Guo, Y. Zhang, L. Sun, K. Zhang, H. Xu, Y. Chen, Checkpoint blockade and nanosonosensitizer-augmented noninvasive sonodynamic therapy combination reduces tumour growth and metastases in mice, Nat. Commun. 10 (2019) 2025–2039.
[20] C. McEwan, J. Owen, E. Stride, C. Fowley, H. Nesbitt, D. Cochrane, C.C. Coussios, M. Borden, N. Nomikou, A.P. McHale, J.F. Callan, Oxygen carrying microbubbles for enhanced sonodynamic therapy of hypoxic tumours, J. Control Release. 203 (2015) 51–56.
[21] Y. Liu, S. Chen, J. Sun, S. Zhu, C. Chen, W. Xie, J. Zheng, Y. Zhu, L. Xiao, L. Hao, Z. Wang, S. Chang, Folate-targeted and oxygen/indocyanine green-loaded lipid nanoparticles for dual-mode imaging and photo-sonodynamic/photothermal therapy of ovarian cancer in vitro and in vivo, Mol Pharm. 16 (2019) 4104–4120.
[22] P. Zhu, Y. Chen, J. Shi, Nanoenzyme-augmented cancer sonodynamic therapy by catalytic tumor oxygenation, ACS Nano. 12 (2018) 3780–3795.
[23] X. Han, J. Huang, X. Jing, D. Yang, H. Lin, Z. Wang, P. Li, Y. Chen, Oxygen-deficient black titania for synergistic/enhanced sonodynamic and photoinduced cancer therapy at near infrared-ii biowindow, ACS Nano. 12 (2018) 4545–4555.
[24] C. Dai, S. Zhang, Z. Liu, R. Wu, Y. Chen, Two-dimensional graphene augments nanosonosensitized sonocatalytic tumor eradication, ACS Nano. 11 (2017) 9467–9480.
[25] J.J. Shi, Z.Y. Chen, B.H. Wang, L. Wang, T.T. Lu, Z.Z. Zhang, Reactive oxygen species-manipulated drug release from a smart envelope-type mesoporous titanium nanovehicle for tumor sonodynamic-chemotherapy, ACS Appl. Mater. Inter. 7 (2015) 28554–28565.
[26] C. Du, Y. Ding, J. Qian, R. Zhang, C.-M. Dong, Dual drug-paired polyprodrug nanotheranostics reverse multidrug resistant cancers via mild photothermal-cocktail chemotherapy, J. Mater. Chem. B. 7 (2019) 5306–5319.
[27] Z. Li, J. Han, L. Yu, X. Qian, H. Xing, H. Lin, M. Wu, T. Yang, Y. Chen, Synergistic Sonodynamic/Chemotherapeutic Suppression of Hepatocellular Carcinoma by Targeted Biodegradable Mesoporous Nanosonosensitizers, Adv. Funct. Mater. 28 (2018) 1800145.
[28] S. Liang, X. Deng, Y. Chang, C. Sun, S. Shao, Z. Xie, X. Xiao, P. Ma, H. Zhang, Z. Cheng, J. Lin, Intelligent hollow Pt-CuS janus architecture for synergistic catalysis-enhanced sonodynamic and photothermal cancer therapy, Nano Lett. 19 (2019) 4134–4145.
[29] Z. Wang, N. Yu, W. Yu, H. Xu, X. Li, M. Li, C. Peng, Q. Wang, M. Zhu, Z. Chen, In situ growth of Au nanoparticles on natural melanin as biocompatible and multifunctional nanoagent for efficient tumor theranostics, J. Mater. Chem. B. 7 (2019) 133–142.
[30] X. Guo, S.G. Chen, Y.Q. Hu, G.Y. Li, N.B. Liao, X.Q. Ye, D.H. Liu, C.H. Xue, Preparation of water-soluble melanin from squid ink using ultrasound-assisted degradation and its anti-oxidant activity, J. Food Sci. Technol. 51 (2014) 3680–3690.
[31] M. Chu, W. Hai, Z. Zhang, F. Wo, Q. Wu, Z. Zhang, Y. Shao, D. Zhang, L. Jin, D. Shi, Melanin nanoparticles derived from a homology of medicine and food for sentinel lymph node mapping and photothermal in vivo cancer therapy, Biomaterials. 91 (2016) 182–199.
[32] Q. Jiang, Z. Luo, Y. Men, P. Yang, H. Peng, R. Guo, Y. Tian, Z. Pang, W. Yang, Red blood cell membrane-camouflaged melanin nanoparticles for enhanced photothermal therapy, Biomaterials. 143 (2017) 29–45.
[33] H. Chen, X. Zhou, Y. Gao, B. Zheng, F. Tang, J. Huang, Recent progress in development of new sonosensitizers for sonodynamic cancer therapy, Drug Discov. Today. 19 (2014) 502–509.
[34] N. Yu, J. Li, Z. Wang, S. Yang, Z. Liu, Y. Wang, M. Zhu, D. Wang, Z. Chen, Blue Te nanoneedles with strong NIR photothermal and laser-enhanced anticancer effects as “all-in-one” nanoagents for synergistic thermo-chemotherapy of tumors, Adv. Healthc. Mater. 7 (2018) 1800643.
[35] Y.L. Liu, K.L. Ai, J.H. Liu, M. Deng, Y.Y. He, L.H. Lu, Dopamine-melanin colloidal nanospheres: An efficient near-infrared photothermal therapeutic agent for in vivo cancer therapy, Adv. Mater. 25 (2013) 1353–1359.
[36] Y. Liu, K. Ai, L. Lu, Polydopamine and its derivative materials: synthesis and promising applications in energy, environmental, and biomedical fields, Chem. Rev. 114 (2014) 5057–5115.
[37] Z. Chen, C. Wu, Z. Zhang, W. Wu, X. Wang, Z.Y. Synthesis, functionalization, and nanomedical applications of functional magnetic nanoparticles, Chinese. Chem. Lett. 29 (2018) 1601–1608.
[38] N. Yu, C. Peng, Z. Wang, Z. Liu, B. Zhu, Z. Yi, M. Zhu, X. Liu, Z. Chen, Dopant-dependent crystallization and photothermal effect of Sb-doped SnO_2 nanoparticles as stable theranostic nanoagents for tumor ablation, Nanoscale. 10 (2018) 2542–2554.
[39] N. Yu, Y. Hu, X. Wang, G. Liu, Z. Wang, Z. Liu, Q. Tian, M. Zhu, X. Shi, Z. Chen, Dynamically tuning near-infrared-induced photothermal performances of TiO_2 nanocrystals by Nb-doping for imaging guided photothermal therapy of tumors, Nanoscale. 9 (2017) 9148–9159.
[40] X.R. Song, X.Y. Wang, S.X. Yu, J.B. Cao, S.H. Li, J. Li, G. Liu, H.H. Yang, X.Y. Chen, Co_9Se_8 nanoplates as a new theranostic platform for photoacoustic/magnetic resonance dual-modal-imaging-guided chemo-photothermal combination therapy, Adv. Mater. 27 (2015) 3285–3291.
[41] A. Liopo, R. Su, A.A. Oraevsky, Melanin nanoparticles as a novel contrast agent for optoacoustic tomography, Photoacoustics. 3 (2015) 35–43.